Low Resistivity Aluminum Doped Layers Formed Using High Dose High Temperature Implants and Laser Annealing

Fulvio Mazzamuto, Zeinab Chehadi, Fabien Roze, Mathieu Opprecht, Atul Gupta, Sébastien Kerdilès, Toshiyuki Tabata, Mike Ameen, Dwight Dongwan Roh, Christina Sohl, et al.

Low resistivity aluminum doped layers formed using high dose high temperature implants and laser annealing

F. Mazzamuto[1,a*], Z. Chehadi[2,b], F. Roze[2], M. Opprecht[3,c], A. Gupta[1], S.Kerdilés[3], T. Tabata[2], M. Ameen[1], D. Roh[1], C.Sohl[1], M. Lazar[4,d], L.Rubin[1],L. Thuries[2]

[1]Axcelis Technologies, Inc., Beverly, MA USA

[2]Laser Systems & Solutions of Europe (LASSE), Gennevilliers, France

[3]Université Grenoble Alpes, CEA LETI, Grenoble, France

[4]L2n, EMR CNRS 7004, UTT, 12 rue Marie Curie CS 42060, 10004 Troyes

[a] fulvio.mazzamuto@axcelis.com, [b] zeinab.chehadi@screen-lasse.com, [c] mathieu.opprecht@cea.fr, [d]mihai.lazar@utt.fr

* corresponding author

Keywords: SiC, Aluminum implantation, high temperature implantation, p-type junction, furnace annealing, laser annealing, carbon capping, damage annealing, dopant activation

Abstract. This paper demonstrates for the first time a new annealing scheme to form p-type junctions in SiC by high temperature ion implantation followed by laser annealing without the use of a protective carbon capping layer. This novel approach leverages higher substrate temperatures during implant to minimize implant-induced defects during ion implantation, which enables the use of reduced thermal budget laser annealing for dopant activation. Laser annealing enables higher surface temperatures in the implanted layer than conventional annealing using a high temperature furnace. The shorter thermal budget results in higher dopant activation while minimizing, the formation of extended defects observed during high thermal budget furnace annealing, which can lead to undesirable degradation in device performance. By using laser annealing with no carbon capping layer, the sheet resistance of the implanted layers is reduced up to 6 times with respect to the conventional process (using a furnace anneal and carbon capping layers).

Introduction

Increasing the activated dopant concentration in the highly doped regions in SiC devices remains a critical area of development as manufacturers drive continued scaling and improved performance in next generation devices. Current SiC devices utilize high dose (typically ≥1e14 at/cm^2) ion implantation processes with substrate temperatures typically at 400-600°C followed by high temperature annealing in a furnace with carbon capping layers [1] to form the highly doped regions of the devices. This process of record (POR) limits the maximum dopant concentration to the range 5×10^{19}–2×10^{20}cm^{-3}[2]. As the implant dose increases, an enhanced level of basal stacking faults (BSF) that grow during post implantation annealing is observed [2] along with a lower activated fraction of the implanted dopant due to an increased concentration of deep level traps [3]. In this work we explore a new approach to deliver higher active concentrations using higher implant temperatures (to reduce the implant induced damage at higher doses) combined with a new laser annealing approach while eliminating the carbon cap. The electrically active dopant concentrations in the implanted junction obtained by the new process flow are compared with those prepared using conventional methods. We explore the interaction of implant damage as a function of dose and implant temperature in combination with annealing.

The proposed new flow brings two potential benefits to SiC manufacturing, 1) the manufacturing is simplified (by eliminating the need for a carbon capping layer prior to anneal), thus reducing manufacturing costs, and 2) the defectivity in the devices (extended defect growth observed in

conventional annealing process [2]) is reduced due to the reduced thermal budget with the laser annealing process. Another potential benefit could be improved dopant activation due to raising the annealing/activation temperature significantly higher than 1700°C [4] without the penalty of increased defectivity. A low thermal budget annealing selective to the surface (enabled via laser annealing) will also prevent any bulk degradation in the devices such as carbon vacancies [5] and offers the flexibility to be integrated at different phases of the manufacturing flow (for instance frontside and backside of the process). This contrasts with a furnace that can only be applied at the beginning of the process where the wafer can sustain the thermal budget.

Successful integration of laser annealing without a carbon capping layer for junction activation has not been previously reported to our knowledge. The short timescale (nanoseconds) of laser annealing is ineffective for damage repair and activation of dopants, thus necessitating either high fluence [6] or multiple irradiation pulses [7,8] to have a positive influence on crystal recovery. However, such intensive irradiation during the laser anneal may result in a crystal reconstruction with structural defects such as the formation of different crystal phases [9] or surface degradation [7]. These negative effects are particularly enhanced in heavily damaged SiC (resulting from high dose implantation at conventional temperatures), and thus have limited the laser annealing approach from adoption for post-implant activation. In this work we mitigate these limitations by (i) optimizing the ion implantation conditions to minimize implant-induced defects and (ii) optimizing the laser annealing conditions by limiting the laser fluence below the damaging threshold and extending the dwell time (microseconds) to maximize the effectiveness.

In the first section, the sample preparation is described, followed by a detailed analysis of the optimized ion implantation. Then the effectiveness of the new laser annealing is compared to conventional process. Finally, the advantages of the junction obtained, the surface morphology, crystal defectivity and electrical characteristics are discussed.

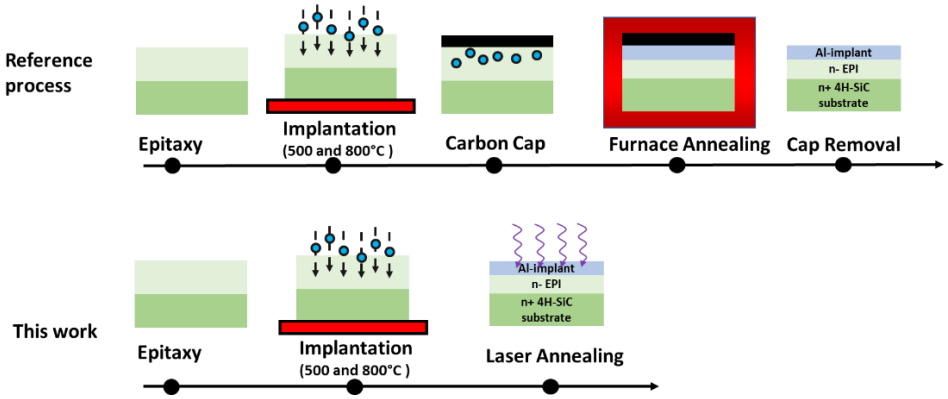

Figure 1: The process sequences used for the preparation of samples. Industrial process (top) refers to the conventional process flow used in manufacturing and is contrasted with this work (bottom) that eliminates the pre anneal deposition and post anneal removal of the carbon capping layer.

Sample preparation

Standard monocrystalline 4H-SiC substrates with a 4° offset of the <0001> axis and an epitaxial layer having a low nitrogen concentration (< 1 ×10^{16} cm^{-3}) were used in this study. All substrates were implanted with aluminum ions at either 500°C or 800°C with the same implant chains to obtain a comparable Al-doped layer, then split into two halves. One half followed the conventional process, while the other half was processed by laser annealing. A schematic of the two process flows is presented in Figure 1. The samples following the conventional process were coated with a sacrificial carbon capping layer and furnace annealed at 1700°C for 30 minutes. The carbon layer was removed before characterization. Furnace annealing conditions selected were typical of those used in manufacturing and determined based on the tradeoff between maximizing dopant activation while

avoiding excessive defect formation during the high thermal budget anneal. Samples following the new process sequence were directly laser annealed without the carbon capping layer.

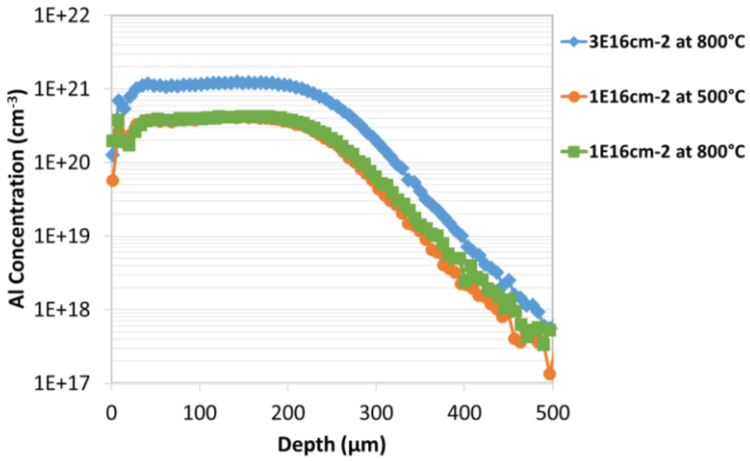

Figure 2: final SIMS profile after ion implantation chain. Energy and dose at both 500°C, equivalent to Negoro et al. [1], and 800°C.

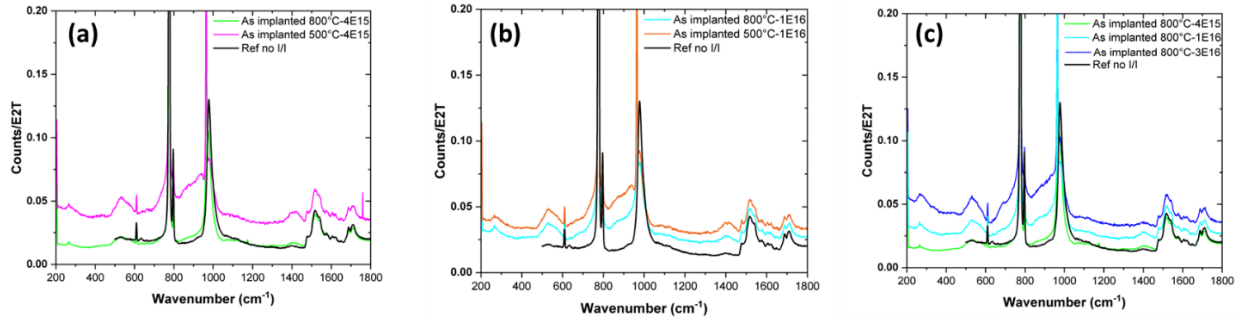

Figure 3: Effect of temperature during implant for lower doses (a), and higher doses (b). (c) Effect of the dose with all samples implanted at 800°C.

Defect modulation by hot temperature ion implantation

The ion implantation was optimized to form a box-like profile with various concentrations of p-type dopant into the n-type doped epitaxial layer grown on a 4H SiC substrate. For each sample, the final aluminum profiles were generated by a sequence of implant sub-steps similar to the one in the Negoro study [1]. Implantation energies and the corresponding ratio of the doses were 160, 100, 60, 30, 10 keV and 0.51, 0.21, 0.15 0.09, 0.04, respectively. Implant profiles are reported in Figure 2. The cumulative dose of Al implants was varied from 4×10^{15} cm^{-2} (a typical range for p+-type junction formation) to doses as high as 3×10^{16} cm^{-2}, which produces a peak concentration above the solid solubility limit of Al in SiC [10]. The same combination of implantation energies and doses were used for all samples, forming a very uniform plateau of Al concentration through 200 nm of depth into the SiC substrate. To assess the impact of temperature on the implant-induced damages, particularly for the highest doses, wafers were implanted at 500°C or 800°C on an Axcelis Purion Power Series implanter. The implant temperature did not show a noticeable change in the Al profile as measured by secondary ion mass spectroscopy (SIMS), as shown in Figure 2 consistent with very low diffusivity of Al in SiC at these temperatures.

Crystal quality after implant and after annealing was measured by Raman spectroscopy using a 473 nm laser probe, expected to be sensitive to implantation-induced defects [11]. Signals obtained were normalized by the E2T peak (776 cm^{-1}) [12] and shown in Figure 3. Measurements before (pristine SiC epitaxial layer) and after ion implantation demonstrate a clear improvement of lattice quality for the sample implanted at 800°C for all doses compared to the ones implanted at 500°C. Fig 3a shows that at the lower total dose of $4\times10^{15}cm^{-2}$, the normalized Raman spectrum of the 800°C

implanted sample is comparable to that of an unimplanted SiC sample. This indicates that the crystal quality is maintained even after implant (i.e. no/little residual damage to the lattice is observed for this high temperature implant condition). In contrast, the sample implanted with the same dose at 500°C shows substantial differences in the Raman signals, suggesting a substantially higher concentration of implant-induced damage. For the higher dose samples (1×10^{16} cm^{-2} reported in Fig 3b), a similar trend is observed: the samples implanted at 800°C show better crystallinity with respect to the ones implanted at 500°C. Finally, Fig 3c compares samples implanted at the same temperature but at different doses. The degree of lattice damage in the implanted samples was observed to increase with the total implanted dose. High temperature Al implantation is expected to boost activation and/or lower the thermal budget requirement of the post-implantation annealing by limiting excess crystal damage [13].

Laser Annealing defect recovery capability

Samples were annealed either by furnace annealing after being capped or by laser annealing without the capping layer. A microsecond UV-laser with a monochromatic wavelength between 300 and 400 nm was used to maximize the light absorption within the implanted layer [11]. Different laser fluences and irradiation times between 1 and 100 µs were used. To avoid the effects of potential SiC dissociation, only conditions in the sub-melt regime were selected for characterization. We initially compared the effectiveness of lattice annealing by using modulated reflectance measurements from a pump and probe laser on a commercially available "Thermawave" (TW) tool from KLA corporation. The TW response is known to be proportional to implant-induced damage in the lattice and is routinely used in Si manufacturing facilities for statistical process control (SPC) on implant steps [14]. TW measurements after annealing and comparison to the unimplanted EPI-SiC substrates allow for a qualitative indication of the lattice damage after implant and after annealing. Figure 4 shows the TW response for all the samples. Despite the significant reduction using higher temperature during implantation, TW response after implantation (Fig 4a) is an order of magnitude higher than after annealing. For the lower doses, the TW response (Fig 4b) for samples both after the furnace or laser anneals are comparable to each other and also to the TW response of unimplanted EPI-SiC samples, indicating nearly complete lattice repair. This suggests that the laser approach, with an annealing time significantly shorter than a furnace, can be as effective as conventional furnace annealing in repairing the lattice damage during high dose implantation. For the highest dose condition ($3\times10^{16}cm^{-2}$), only the long thermal budget of furnace annealing seems to be able to effectively anneal out the excessive implant induced defects. However, this is only a qualitative indication of point defects and does not quantify major extended defects.

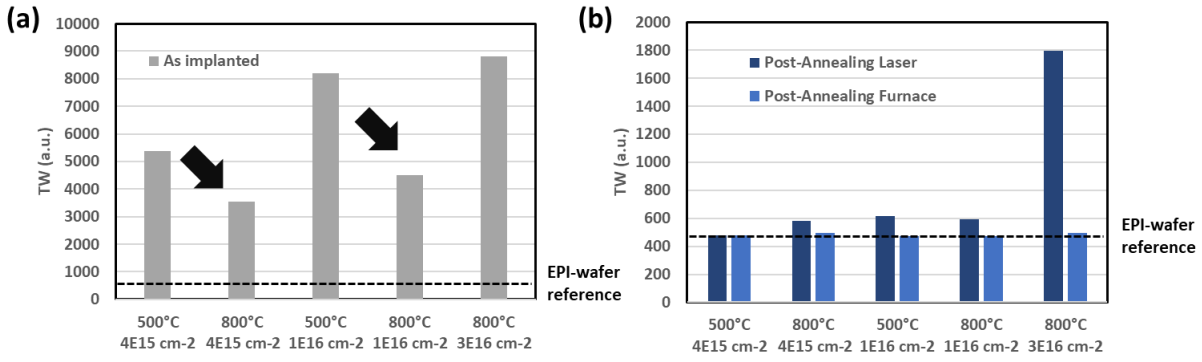

Figure 4: ThermaWave response of all the implanted samples after activation annealing.

Defect recovery by laser annealing was further studied by Raman spectroscopy (Fig. 5). In Figure 5a, for dose $1\times10^{16}cm^{-2}$, the crystal can be perfectly annealed with the crystal quality being

comparable to the EPI-only sample. Beyond $1\times10^{16}cm^{-2}$ (Fig. 5b), laser annealing still anneals out most of the lattice defects though not completely and furthermore the defect levels appear to decrease proportionately with laser irradiation (dwell) times.

The difference between the two processes is most noticeable when looking at the cross-sectional transmission electron microscopy (TEM) images of the annealed layers. Figure 6 compares the TEM images of the implanted layer from the sample with $3\times10^{16}cm^{-2}$ dose after ion implantation step (Fig. 6a), after laser annealing (Fig. 6b) and after furnace annealing (Fig. 6f). The insets of the three images show how the SiC crystallinity is maintained, however in the furnace annealing sample, the implant-induced defects have time to evolve into large extended defects such as basal plane dislocations or polygonal loops. In contrast, the ultra-fast annealing time of the laser prevents this phenomenon. To ensure that laser annealing without any capping layer has not induced any substantial surface degradation, Energy-Dispersive X-Ray (EDX) maps for carbon, aluminum and silicon for the as implanted (Fig. 6c) and laser annealed (Fig. 6d) samples are shown. No noticeable difference before and after the laser annealing indicates that these conditions have not altered the material stoichiometry as frequently observed in previous work [6,9]. In contrast, the EDX maps for the furnace annealed sample (Fig. 6e) show aluminum and carbon precipitates in addition to the extended crystal defects.

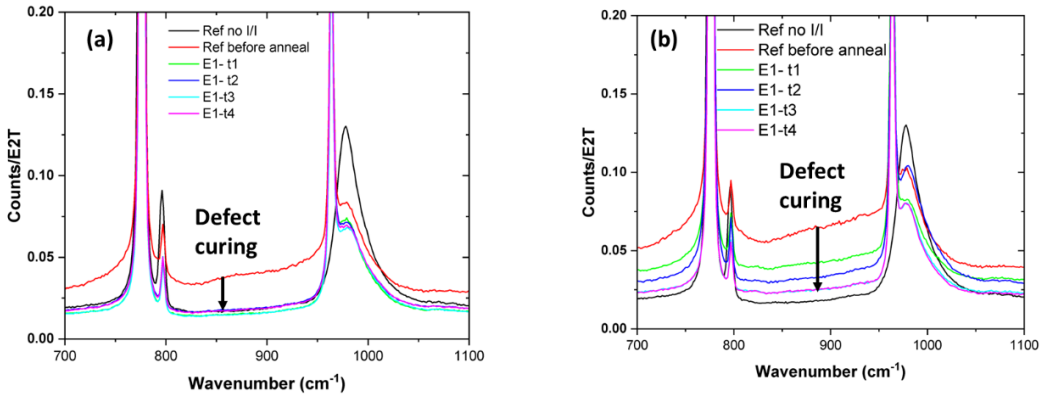

Figure 5: Raman spectrum of the sample after annealing for different laser dwell t, on sample $1\times10^{16}cm^{-2}$ at 800°C (a) and sample $3\times10^{16}cm^{-2}$ at 800°C (b). Dwell time varying from minimum t_1 to maximum t_4.

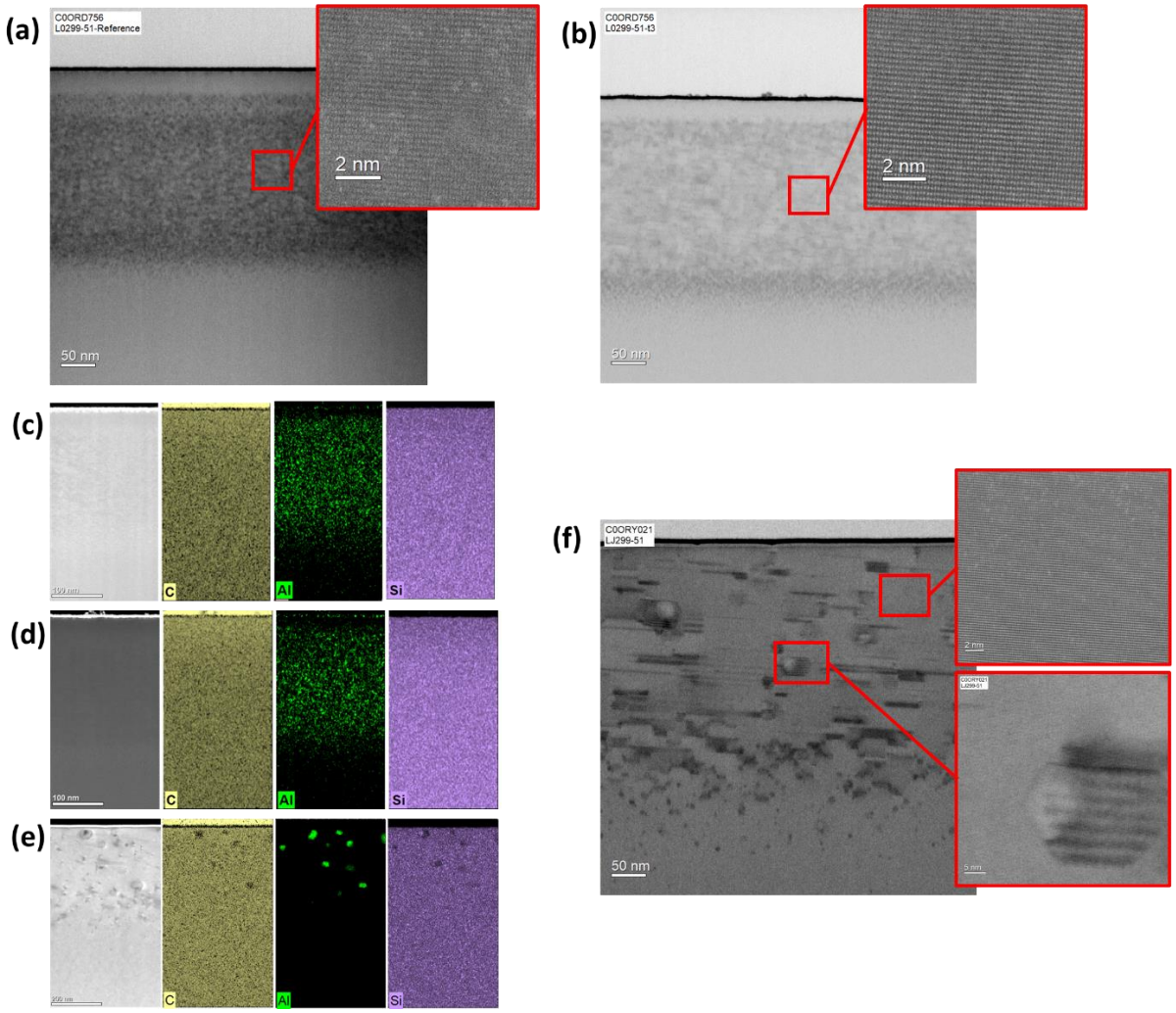

Figure 6: Cross-sectional TEM and EDX images for the samples $3\times10^{16}cm^{-2}$ (a) TEM after ion implantation, (b) TEM after laser annealing (c) EDX map of the same sample after ion implantation, (d) EDX of sample after laser annealing, (e) EDX of sample after furnace annealing and (f) TEM after furnace annealing

Junction formation

Finally, Al activation has been confirmed by sheet resistance, scanning microwave microscopy (SMM, not shown) and scanning capacitance microscopy (SCM) measurements. The sheet resistance (Rs) of all samples were measured by the standard four-point probe method to estimate the electrical performance and a comparison between the process conditions. Rs decreases with the laser irradiation time (not shown) for all implant conditions, indicating that there is an optimal thermal budget that maximizes Al activation without degrading the surface. The Rs for optimum irradiation time is reported for all implant conditions in Figure 7. The measured Rs values are noticeably lower than previously reported data [1] and up to 6 times lower than the sister sample that was furnace annealed (with a capping layer).

The higher resistance of the furnace annealed samples could be due to furnace annealing curing point defects as demonstrated by the low TW values, while the aluminum concentration, above the solubility limit, precipitates into inactive clusters (Fig 6e). This results in an overall lower doping activation rate. The resistance trends and related fundamental mechanisms for laser annealing samples are more complex and will require a dedicated study. We assume that the timescale of the laser process is too short to induce noticeable Al precipitates, which is why the sheet resistance decreases consistently with dose even though the solubility limit is exceeded. Residual defects (for

extreme Al doses) uncured by the reduced thermal budget of the laser process seems to not influence the resistance trends, but their impact has to be considered in a real device.

Figure 7 shows representative SCM images for the lowest Rs. SCM technic provides only a qualitative indication of the carrier type and concentration. Here it demonstrates the obvious formation of an active p-type junction on the n-type EPI layer. The trend shows that the combination of high dose, hot implantation and laser annealing may enable higher performance transistors by enabling lower resistivity in highly doped layers.

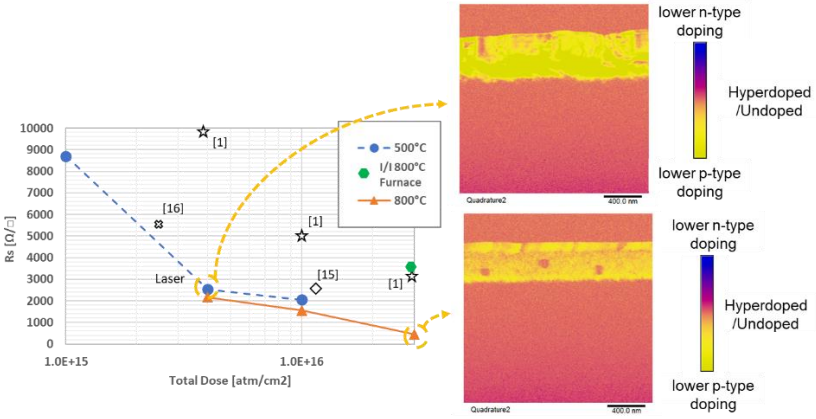

Figure 7: Sheet resistance trends for this work, ion implantation at 500°C and 800°C and optimized laser annealing conditions. On the right, SCM images for two representative points at ultra-low Rs.

Summary

We demonstrate the viability of replacing furnace annealing to form junctions in SiC with a simpler alternative process flow that enables the elimination of a carbon capping layer deposited before anneal and removed post anneal. The alternative process uses higher temperature ion implantation that minimizes lattice damage followed by optimized laser annealing without the carbon capping layer that is required for furnace annealing. The limited crystal degradation due to the 800°C implant allows a simplified integration scheme and optimization of the laser annealing process to maximize activation without inducing the surface degradation observed in prior reports using laser annealing of SiC substrates or the extended defects observed for high thermal budget annealing.

References

[1] Y. Negoro et al. *J. Appl. Phys.*, 96(9), 4916-4922 (2004).

[2] R. Nipoti et al. *Materials Science in Semiconductor Processing*, 78, 13-21 (2017).

[3] G. Pensl et al. *Microelectronic Engineering*, 83(1), 146-149 (2006)

[4] R. Nipoti et al. *Materials Science Forum*, Vol. 924, pp. 333-338, (2018).

[5] H. M. Ayedh, et al. *J. Appl. Phys.*, 115.1 (2014).

[6] F. Mazzamuto et al. *Materials Science Forum*. Vol. 858. (2016).

[7] C. Calabretta et al. *Materials* 12.20, 3362 (2019).

[8] C. Calabretta et al. *Materials Science Forum*. Vol. 1062 (2022).

[9] M. Vivona et al. *ACS Applied Electronic Materials*, *4*(9), 4514-4520 (2022).

[10] Y. Tajima et al. *J. American Ceramic Society* 65.2, C-27 (1982).

[11] I. G. Atabaev et al. *Journal of Spectroscopy* (2018).

[12] Q. Jia et al. *Appl. Phys. Lett*. 112(19), 192102 (2018)

[13] N. S. Saks et al. *Appl. Phys. Lett*. 84, 5195 (2004)

[14] S. Wurn et al. *Appl. Phys. A* 47(2) :147-155 (1988)

[15] S. G. Sundaresan et al. *J. Appl. Phys* 101(7), 073708 (2007).

[16] R. Nipoti et al. *Materials Science Forum*, Vol. 924, pp. 333-338 (2018)